

# 3-D FDTD Modeling of Electromagnetic Wave Propagation in Magnetized Plasma Requiring Singular Updates to the Current Density Equation

Santosh Pokhrel<sup>✉</sup>, Student Member, IEEE, Varun Shankar, and Jamesina J. Simpson, Senior Member, IEEE

**Abstract**—A new finite-difference time-domain (FDTD) algorithm for electromagnetic wave propagation in magnetized plasma is proposed. This algorithm permits the use of two time step increments: one for Maxwell’s equations,  $\Delta t$ , and the other for the current density equation derived from the Lorentz equation of motion,  $\Delta t_c$ . A major advantage of this algorithm over previous approaches is that only a single update iteration is needed for the current density equation even when  $\Delta t_c < \Delta t$ . This provides significant time savings that can make previously infeasibly long simulations now practical. The algorithm’s implementation is also relatively simple and it has relatively low memory requirements. The algorithm is validated against analytical results. A stability analysis is performed.

**Index Terms**—Earth, earth-ionosphere waveguide, electromagnetic (EM) wave propagation, finite-difference time-domain (FDTD), ionosphere, plasma.

## I. INTRODUCTION

LECTROMAGNETIC wave propagation through or reflected by magnetized ionospheric plasma is an important aspect of long-range radio communications, satellite communications, geolocation, over-the-horizon radar, propagation from lightning, and so on. Over the last couple of decades, finite-difference time-domain (FDTD) [1], [2] models have been developed to model electromagnetic (EM) wave propagation in both nonmagnetized (isotropic) and magnetized (anisotropic) plasmas [3]–[14]. Although more computationally demanding than ray-tracing and mode theory approaches, FDTD provides the ability to model detailed and more realistic spatial variations in the electron (and ion) densities and collision frequencies. Furthermore, FDTD can model complex and wideband source time-waveforms.

Of particular interest in this paper is the ability to model EM wave propagation in the Earth–ionosphere waveguide in fully 3-D, on a global scale, and at high resolutions (on the order of  $\sim 1$  km and higher) [15]–[18]. Previously, a parallelization

Manuscript received January 5, 2018; revised May 4, 2018; accepted May 31, 2018. Date of publication June 14, 2018; date of current version August 31, 2018. This work was supported by the National Science Foundation under Grant 1662318. (Corresponding author: Santosh Pokhrel.)

S. Pokhrel and J. J. Simpson are with the Electrical Engineering Department, The University of Utah, Salt Lake City, UT 84112 USA (e-mail: santosh\_everest@yahoo.com).

V. Shankar is with the Department of Mathematics, The University of Utah, Salt Lake City, UT 84112 USA (e-mail: vshankar@math.edu).

Color versions of one or more of the figures in this paper are available online at <http://ieeexplore.ieee.org>.

Digital Object Identifier 10.1109/TAP.2018.2847601

scheme [19] and a parallel I/O methodology [20] were developed for such models. Including magnetized ionospheric plasma using previously published algorithms, however, results in long simulation times that render many simulations impractical. For the first time, two drastic time-saving developments now render many such simulations practical: 1) the first development was provided by [5], which introduces the use of two time step increments (one for Maxwell’s equations and the other for the current density equation); this feature is retained in the algorithm proposed in this paper; and 2) the second development is introduced by the algorithm in this paper (singular updates to the current density equation for every Maxwell’s equations updates). The combination of above-mentioned developments 1 and 2 greatly expands the modeling capabilities of global 3-D FDTD modeling at high resolutions by significantly reducing the required simulation times.

Expanding on above-mentioned development 1, Samimi and Simpson [5] proposed an efficient 3-D FDTD model of EM wave propagation in magnetized plasma by employing Boris’s algorithm [21], which was previously applied to particle-in-cell plasma models. The algorithm of [5] requires less memory than the previous approaches and also provides flexibility in choosing two time step increments: one for Maxwell’s equations,  $\Delta t$ , and the other for the current density equation (derived from the Lorentz equation of motion),  $\Delta t_c$ . This is helpful when modeling high collision frequencies, which leads to a reduced  $\Delta t_c$  relative to  $\Delta t$  by the factors of 10 or 100 or more.

We note that several other 2-D cylindrically symmetric [22], [23] and fully 3-D FDTD magnetized plasma algorithms have been proposed [3], [4], [6]–[14]. However, all but one of these models to-date have time step increments that are tied to the plasma. Lee and Kalluri [12], for example, place all of the current density vectors ( $J_x$ ,  $J_y$ , and  $J_z$ ) at the center of the Yee cell to maintain symmetry in the grid (the proposed method in this paper also collocates the current density vectors). However, the required time step using the methodology of [12] is very small at low altitudes. Furthermore, the algorithm in [12] does not permit the use of two time stepping schemes.

Reference [13] uses the discontinuous Galerkin finite-element time-domain method and [14] uses the higher order locally corrected Nystrom time-domain volume-integral equation method to solve for EM wave propagation in an

anisotropic plasma medium. However, the memory costs are much higher for higher order methods. Furthermore, determining the stability conditions may be extremely challenging for these methods.

The one model proposed to-date that has a numerical stability condition independent of the plasma parameters is the direct integration method of [6]. Using this approach, only the stability condition for Maxwell's equations must be satisfied. However, the method is very memory intensive. There are more than 24 update equations for the magnetic field intensity,  $\vec{H}$ , electric field intensity,  $\vec{E}$ , and plasma current density,  $\vec{J}$ , whereas only nine update equations are required in other magnetized plasma models [3]–[5]. As a result, the methodology of [6] is infeasible for large 3-D modeling scenarios due to the large memory requirements. The method of [6] also employs a nontraditional grid cell as a template (instead of the Yee cell) with all three components of  $\vec{E}$  and  $\vec{H}$  at each node of the grid (a nonstaggered grid).

In this paper, the current density equation is derived from the Lorentz equation of motion (see Section II) in a way that minimizes the memory requirements while retaining the possibility of using two time step increments as in [5] ( $\Delta t$  and  $\Delta t_c$ ). The algorithm is further developed to require only one update at each time step for the current density equation even when  $\Delta t_c \ll \Delta t$ . Next, a complete stability analysis is performed on the current density update equation, and several stability conditions are suggested in Section III. The performance of the model is then compared with previous approaches in Section IV. Finally, the algorithm is validated against several plasma analytical theory results in Appendix B.

## II. METHODOLOGY

### A. Governing Equations

The governing equations are as follows:

$$\nabla \times \vec{E} = -\frac{\partial \vec{B}}{\partial t} \quad (\text{Faraday's Law}) \quad (1)$$

$$\nabla \times \vec{H} = \frac{\partial \vec{D}}{\partial t} + \sum \vec{J}_j + \vec{J}_s \quad (\text{Ampere's Law}) \quad (2)$$

$$\frac{\partial \vec{J}_j}{\partial t} + v_j \vec{J}_j = \varepsilon w_{pj}^2 \vec{E} - \vec{w}_{cj} \times \vec{J}_j \quad (\text{Current Density Equation}) \quad (3)$$

where  $J_s$  is the source current density,  $J_j$  represents the plasma current density due to each  $j$ -species (the subscript  $j$  represents electrons, positive ions, and so on.),  $v_j$  represents the collision frequency,  $\varepsilon$  is the electrical permittivity of the medium,  $w_{pj}$  is the angular frequency of plasma, and  $w_{cj}$  is the cyclotron frequency.

### B. Derivation of the Update Equations

For convenience, the algorithm presented in this paper is in Cartesian coordinates. It may be adapted to spherical coordinates as needed as is done in [4] and [5]. Following the traditional FDTD method, the  $\vec{E}$  and  $\vec{H}$  fields are staggered in both space and time as

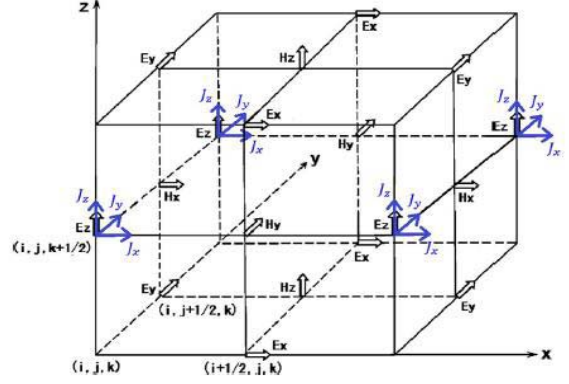


Fig. 1. FDTD grid cell showing the spatial positions of the electric field, magnetic field, and current density vectors.

shown in Fig. 1. Furthermore, (1) and (2) are solved using a time step increment ( $\Delta t$ ), such that  $\Delta t < (1/c)(1)/(\sqrt{(1/\Delta x^2) + (1/\Delta y^2) + (1/\Delta z^2)})$  is satisfied (the Courant Friedrichs Lewy (CFL) limit [2]). The spatial resolutions in the  $x$ -,  $y$ - and  $z$ -directions of the grid are  $\Delta x$ ,  $\Delta y$ , and  $\Delta z$ , respectively.

An appropriate update equation for the  $J_j$  components must be determined. To do this, (3) is first analyzed stepwise with an eigenvalue calculation. If the eigenvalue is a negative real number, the current density equation should be solved using an implicit technique. If the eigenvalue is complex, the equation should be solved explicitly.

First, the eigenvalue is calculated for the first-order time derivative in (3)

$$\frac{\partial J_j}{\partial t} = \lambda J_j \quad (\lambda \text{ is the assumed eigenvalue})$$

Let  $J_j = |J_j|e^{-imt}$ , then

$$\frac{\partial J_j}{\partial t} = (-im)|J_j|e^{-imt} = (-im)J_j$$

And,  $\lambda = (-im)$ .

From the above-mentioned analysis, the first term of (3) (the time derivative of  $J_j$ ) has an imaginary eigenvalue. The second and third terms,  $v_j \vec{J}_j$  and  $\varepsilon w_{pj}^2 \vec{E}$ , are the linear terms that only rescale the magnitude of the vector fields. The term  $\vec{w}_{cj} \times \vec{J}_j$  includes the curl operator that rotates the vector orientation (orthogonal to both  $w_{cj}$  and  $J_j$ ). None of these other terms have negative real eigenvalues. Therefore, all the terms in (3) will be solved using an explicit technique.

The  $\vec{w}_{cj} \times \vec{J}_j$  term is nonlinear. This can be solved by expanding the following matrix:

$$\begin{bmatrix} \vec{i} & \vec{j} & k \\ w_x & w_y & w_z \\ J_x & J_y & J_z \end{bmatrix}$$

to yield

$$= \vec{i} (w_y J_z - w_z J_y) + \vec{j} (w_z J_x - w_x J_z) + \vec{k} (w_x J_y - w_y J_x).$$

The above expression can be written in matrix form as

$$\begin{bmatrix} 0 & -wz & wy \\ wz & 0 & -wx \\ -wy & wx & 0 \end{bmatrix} \begin{bmatrix} J_x \\ J_y \\ J_z \end{bmatrix}$$

The above matrix is written symbolically as  $[Q]_{3 \times 3} [J_j]_{3 \times 1}$ .

Now, discretizing (3) yields the following:

$$\begin{aligned} \frac{J_j^{n+\frac{1}{2}} - J_j^{n-\frac{1}{2}}}{\Delta t_c} + v_j \frac{J_j^{n+\frac{1}{2}} + J_j^{n-\frac{1}{2}}}{2} \\ = \epsilon w_{pj}^2 \vec{E}_n - [Q] \frac{J_j^{n+\frac{1}{2}} + J_j^{n-\frac{1}{2}}}{2} \end{aligned} \quad (4)$$

where  $\Delta t_c$  is the time step increment for the current density terms [which may be different from the  $\Delta t$  time step increment used to update (1) and (2)]. Moving all of the future plasma current density terms to the left-hand side of the equation yields

$$\begin{aligned} \left( [I] + [I] \frac{v_j \Delta t_c}{2} + \frac{[Q] \Delta t_c}{2} \right) J_j^{n+\frac{1}{2}} \\ = \epsilon \Delta t_c \cdot w_{pj}^2 \cdot \vec{E}_n + \left( [I] - [I] \frac{v_j \Delta t_c}{2} - \frac{[Q] \Delta t_c}{2} \right) J_j^{n-\frac{1}{2}} \end{aligned} \quad (5)$$

where  $[I]$  is an identity matrix of order  $3 \times 3$ . Let  $a = (1 + (v_j \Delta t_c)/2)$  and  $b = (1 - (v_j \Delta t_c)/2)$ . Then, (5) is expanded as follows:

$$\begin{aligned} & \begin{bmatrix} a & -\frac{\Delta t_c}{2} \omega_z & \frac{\Delta t_c}{2} \omega_y \\ \frac{\Delta t_c}{2} \omega_z & a & -\frac{\Delta t_c}{2} \omega_x \\ -\frac{\Delta t_c}{2} \omega_y & \frac{\Delta t_c}{2} \omega_x & a \end{bmatrix} \begin{bmatrix} J_x \\ J_y \\ J_z \end{bmatrix}^{n+\frac{1}{2}} \\ & = \epsilon \Delta t_c \cdot w_{pj}^2 \begin{bmatrix} Ex \\ Ey \\ Ez \end{bmatrix}^n \\ & + \begin{bmatrix} b & \frac{\Delta t_c}{2} \omega_z & -\frac{\Delta t_c}{2} \omega_y \\ -\frac{\Delta t_c}{2} \omega_z & b & \frac{\Delta t_c}{2} \omega_x \\ \frac{\Delta t_c}{2} \omega_y & -\frac{\Delta t_c}{2} \omega_x & b \end{bmatrix} \begin{bmatrix} J_x \\ J_y \\ J_z \end{bmatrix}^{n-\frac{1}{2}}. \end{aligned} \quad (6)$$

The  $3 \times 3$  order matrix on the left- and right-hand sides of (6) are replaced with matrices  $[A]$  and  $[B]$  in (7), which solves for the future current density terms. For convenience, the matrices are also shown in Appendix A

$$\begin{bmatrix} J_x \\ J_y \\ J_z \end{bmatrix}^{n+\frac{1}{2}} = \epsilon \cdot \Delta t_c \cdot w_{pj}^2 \cdot [A^{-1}]_{3 \times 3} \cdot \begin{bmatrix} Ex \\ Ey \\ Ez \end{bmatrix}^n + [A^{-1}]_{3 \times 3} \cdot [B]_{3 \times 3} \cdot \begin{bmatrix} J_x \\ J_y \\ J_z \end{bmatrix}^{n-\frac{1}{2}}. \quad (7)$$

In (7), if  $\Delta t_c > \Delta t$  (based upon stability criteria given in Section III),  $\Delta t_c$  can be replaced by  $\Delta t$  to make the lapsed real-time consistent with (1) and (2). If  $\Delta t_c < \Delta t$ , the coefficient matrices of (7) may be rederived to permit the

current density vector components to be updated using a single update equation. This is shown in Section II-C.

As mentioned earlier, the  $\vec{E}$  and  $\vec{H}$  field vectors are spatially staggered in the Yee cell of Fig. 1. As it is done in previous approaches [22], the current density vectors ( $J_x$ ,  $J_y$ , and  $J_z$ ) are collocated with an electric field component (here chosen to be the electric field oriented in the  $z$ -direction,  $E_z$ ). This arbitrary choice of collocating the current density vectors with one electric field component ( $E_z$ ) does not introduce additional error since spatial averaging is required regardless of the chosen position for the current density vectors. The current density vectors could also be placed symmetrically at the center of the Yee cell as in [12]. This may simplify the updates along material and domain boundaries.

While solving Ampere's law (2) with  $J$ 's collocated with  $E_z$ , the current density vectors are needed at the location of the electric field vectors (i.e.,  $J_x$  is needed at the location of  $E_x$ , and  $J_y$  and  $J_z$  are needed at the position of  $E_y$  and  $E_z$ , respectively.) Since  $J_x$  is not located at the same position as  $E_x$ , as shown in Fig. 1, spatial averaging is needed to correct the spatial position of  $J_x$ . Similarly, spatial averaging is needed for  $J_y$ . Spatial averaging is achieved by averaging the four nearest neighbors to the location of interest. This process has been successfully used in previous algorithms [3]–[5]

$$\begin{aligned} J_x(i + 1/2, j, k) = & (J_x(i, j, k + 1/2) + J_x(i, j, k - 1/2) \\ & + J_x(i + 1, j, k + 1/2) \\ & + J_x(i + 1, j, k - 1/2))/4 \end{aligned} \quad (8)$$

$$\begin{aligned} J_y(i, j + 1/2, k) = & (J_y(i, j, k + 1/2) + J_y(i, j, k - 1/2) \\ & + J_y(i, j + 1, k + 1/2) \\ & + J_y(i, j + 1, k - 1/2))/4. \end{aligned} \quad (9)$$

Spatial averaging is not needed for  $J_z$  since it is already positioned at the location of  $E_z$ .

Similarly, while solving the Lorentz equation of motion (3), the electric vectors ( $E_x$  and  $E_y$ ) are needed at the location of current density positions ( $J_x$  and  $J_y$ ), respectively

$$\begin{aligned} E_x(i, j, k + 1/2) = & (E_x(i + 1/2, j, k) + E_x(i - 1/2, j, k) \\ & + E_x(i + 1/2, j, k + 1) \\ & + E_x(i - 1/2, j, k + 1))/4 \end{aligned} \quad (10)$$

$$\begin{aligned} E_y(i, j, k + 1/2) = & (E_y(i, j + 1/2, k) + E_y(i, j - 1/2, k) \\ & + E_y(i, j + 1/2, k + 1) \\ & + E_y(i, j - 1/2, k + 1))/4. \end{aligned} \quad (11)$$

The nine resulting equations (three electric field component updates, three magnetic field component updates, and three current density component updates) are solved in a leapfrog manner. The electric field vector components ( $E_x$ ,  $E_y$ , and  $E_z$ , as shown in Fig. 1) are solved at integer time steps,  $n$ , and the magnetic field vector components ( $H_x$ ,  $H_y$ , and  $H_z$ ) and the current density components ( $J_x$ ,  $J_y$ , and  $J_z$ ) are solved at one and a half time step later (at  $n + (1/2)$ ).

### C. Current Density Update Equation When $\Delta t_c < \Delta t$

When  $\Delta t_c < \Delta t$ , (3) must be updated more times than (1) and (2) over the same time span of interest.

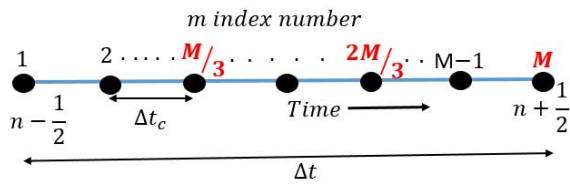


Fig. 2. Updating the  $J$  M times between  $n - (1/2)$  and  $n + (1/2)$ .

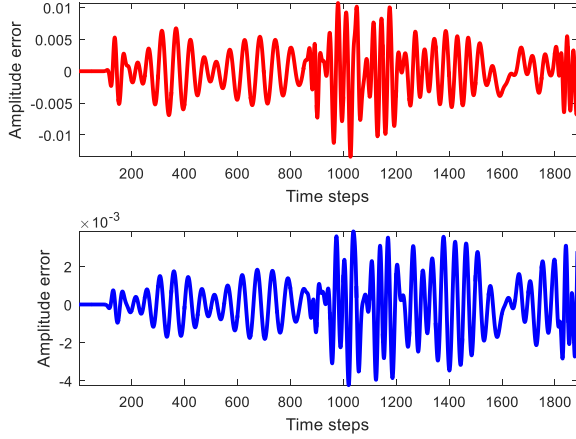


Fig. 3. Top: relative error between the two modeling scenarios: 1) the brute-force approach of lowering  $\Delta t$  to match  $\Delta t_c$ , i.e.,  $\Delta t = \Delta t_c = 19.05$  fs and 2) setting  $(\Delta t_c = (\Delta t)/100) = (1.905 \text{ ps}/100) = 19.05$  fs) and using a singular update of  $\vec{J}$ . Bottom: relative error between the same two scenarios, as in the top, but for 2 using three updates of  $\vec{J}$  rather than one over each  $\Delta t$ .

It is advantageous to be able to update (3) the same number of times as (1) and (2) to speed up the computation, especially since  $\Delta t_c$  can sometimes be 10 or even 100 times smaller than  $\Delta t$ .

In this case, (7) can be rewritten as

$$[J]_{3 \times 1}^{n+\frac{1}{2}} = [K]_{3 \times 1} + [C]_{3 \times 3} \cdot [J]_{3 \times 1}^{n-\frac{1}{2}} \quad (12)$$

where

$$\begin{aligned} [J]_{3 \times 1}^{n+\frac{1}{2}} &= \begin{bmatrix} J_x \\ J_y \\ J_z \end{bmatrix}^{n+\frac{1}{2}} \\ [K]_{3 \times 1} &= \varepsilon \cdot \Delta t_c \cdot w_{pj}^2 \cdot [A^{-1}]_{3 \times 3} \cdot \begin{bmatrix} E_x \\ E_y \\ E_z \end{bmatrix}^n \\ [C]_{3 \times 3} &= [A^{-1}]_{3 \times 3} \cdot [B]_{3 \times 3}. \end{aligned}$$

For instance, if  $\Delta t_c = (\Delta t/M)$ , the current density ( $J$ ) should be updated  $M$  times between  $n - (1/2)$  and  $n + (1/2)$ , as shown in Fig. 2.

For each of the  $M$  updates in Fig. 2, the  $[K]$  matrix remains unchanged since the same electric field values from time step  $n$  are used for all the updates. The error is around 1% with this assumption, as shown in Fig. 3 (top). Similarly, the  $[C]$  matrix remains constant as it is time independent.

In the following derivation,  $[J]_{3 \times 1}^{n-(1/2)}$  (the  $J$  array at  $m = 1$ , as shown in Fig. 2) is written as  $[J_1]$  for notational simplicity (where 1 stands for the  $m$  number). This notation continues

for each  $m$  update until  $[J_M]$  (representing  $[J]_{3 \times 1}^{n+(1/2)}$ ). Then,

$$[J_2] = [K] + [C] \cdot [J_1] \quad (13)$$

$$[J_3] = [K] + [C] \cdot [J_2]. \quad (14)$$

Substituting (13) into (14) yields

$$[J_3] = [K] + [C] \cdot [J_2] = [K] + [C] \cdot ([K] + [C] \cdot [J_1])$$

$$[J_3] = [K] + [C][K] + [C]^2[J_1]. \quad (15)$$

Note that  $[K]$  and  $[C]$  are calculated using  $\Delta t_c$  as the time step. Continuing until the  $M$ th update

$$[J_M] = [K] + [C][K] \dots + [C]^{M-1}[J_1]. \quad (16)$$

Taking  $[K]$  from all but the last term yields

$$\begin{aligned} [J_M] &= ([I] + [C] + [C]^2 \dots [C]^{M-2}) \\ &\quad \cdot [K] + [C]^{M-1}[J_1] \end{aligned} \quad (17)$$

where  $[I]$  is an identity matrix of order 3.

The final form of the update equation is given follows:

$$\begin{aligned} \begin{bmatrix} J_x \\ J_y \\ J_z \end{bmatrix}^{n+\frac{1}{2}} &= ([I]_{3 \times 3} + \sum_{k=1}^{M-2} ([A^{-1}]_{3 \times 3} [B]_{3 \times 3})^k) \cdot \varepsilon \cdot \Delta t_c \\ &\quad \cdot \omega_{pj}^2 \cdot [A^{-1}]_{3 \times 3} \cdot \begin{bmatrix} E_x \\ E_y \\ E_z \end{bmatrix}^n \\ &\quad + ([A^{-1}]_{3 \times 3} [B]_{3 \times 3})^{M-1} \cdot \begin{bmatrix} J_x \\ J_y \\ J_z \end{bmatrix}^{n-\frac{1}{2}} \end{aligned} \quad (18)$$

where  $M = \Delta t / \Delta t_c$ . When  $\Delta t_c < \Delta t$ , everything presented in Section II-B remains the same except that the current density vectors are updated using (18) rather than (7).

Similar to [12], the algorithm proposed in this paper also permits the use of time-varying magnetized plasma parameters. The memory requirements are discussed in detail in Section IV.

#### D. Current Density Update Equation When $\Delta t_c < \Delta t$ With Three Updates of $\vec{J}$

For certain applications requiring high accuracy, the above-presented algorithm may be slightly modified. Instead of assuming constant electric field values over the full  $\Delta t$  for the current density updates, the electric field may be extrapolated using the Lagrange polynomials to discrete points (such as points  $(2M/3)$  and  $M$ , as shown in Fig. 2) using electric field values at time step  $n$  and  $n - 1$ . Higher order Lagrange polynomials would be more accurate; however, electric field values at additional previous time step increments will be needed. This may be very memory intensive for larger simulations. Therefore, an example of first-order extrapolation is shown in this paper.

The current density vector at point  $(M/3)$  in Fig. 2 should be evaluated using the electric field at time step  $n$ . Then, the current density vector at point  $(2M/3)$  and  $n + (1/2)$  time step should be determined using extrapolated electric field values. Therefore, the current density vectors are updated three times

TABLE I  
VALUES USED IN (19)

Value of 'a'	Electric field	Value of 'b'	Points (in Fig. 2)
1/3	$[E]^n$	0	$M/3$
2/3	$\frac{4}{3}[E]^n - \frac{1}{3}[E]^{n-1}$	1/3	$2M/3$
1	$\frac{5}{3}[E]^n - \frac{2}{3}[E]^{n-1}$	2/3	$M$

for every update of the electric and magnetic field components. In this case, (18) changes to

$$\begin{bmatrix} J_x \\ J_y \\ J_z \end{bmatrix}^{n-\frac{1}{2}+a} = \left( [I]_{3 \times 3} + \sum_{k=1}^{M/3-2} ([A^{-1}]_{3 \times 3} [B]_{3 \times 3})^k \right) \cdot \epsilon \cdot \Delta t_c \cdot \omega_{pj}^2 \cdot [A^{-1}]_{3 \times 3} \cdot \begin{bmatrix} Ex \\ Ey \\ Ez \end{bmatrix}_{\text{extrapolated}} + ([A^{-1}]_{3 \times 3} [B]_{3 \times 3})^{M/3-1} \cdot \begin{bmatrix} J_x \\ J_y \\ J_z \end{bmatrix}^{n-\frac{1}{2}+b}. \quad (19)$$

The values of "a" and "b" and the extrapolated electric field are given in Table I.

Using (19) as the update equation, the error decreases to below 0.5%, as shown in Fig. 3 (bottom). The computational savings using this approach are described in Section III, and the increase in memory requirements is discussed in Section IV.

### III. TIME SAVINGS AND STABILITY ANALYSIS

The algorithm of Section II is validated in Appendix B.

#### A. Time Savings

The effect of using two time step increments is tested: 1) setting  $\Delta t_c$  to a lower value than  $\Delta t$  ( $\Delta t_c = \Delta t/100$ ) and using fewer  $\vec{J}$  updates and 2) the brute-force approach of lowering  $\Delta t$  to match  $\Delta t_c$  ( $\Delta t_c = \Delta t$ ). This test is run for whistler-mode propagation in plasma, as shown in Fig. 6. As shown in Fig. 3 (top), the error between the two cases is below 1% throughout the simulation when a singular update of  $\vec{J}$  every  $\Delta t$  is used. However, the error decreases to less than 0.5% when using three updates of  $\vec{J}$  at every  $\Delta t$ . The error will further decrease as more updates of  $\vec{J}$  are used between every  $\Delta t$  but it comes at the cost of higher computational resources. As a result, the level of error may be controlled based on the user needs and computational limitations.

A second test case (same simulation domain as in Appendix B1) is run for 1000 step to test the speedup between: 1) lowering  $\Delta t$  to match  $\Delta t_c$  so that only one time step increment value is used (a brute-force approach);

2) setting  $\Delta t_c$  to a lower value than  $\Delta t$  but updating the  $\vec{J}$  components  $m$  times (100 times in this test case) each time step (as for the algorithm of [5]); 3) setting  $\Delta t_c$  to a lower value than  $\Delta t$  while using a single update for the  $\vec{J}$  components (which is permitted by the algorithm of this paper); and 4) setting  $\Delta t_c$  to a lower value than  $\Delta t$  and using three updates for  $\vec{J}$  rather than one. It took 13.35 s for scenario 1, 5.6 s for scenario 2, 0.43 s for scenario 3, and 0.58 s for scenario 4.

The case of  $\Delta t_c = (\Delta t/100)$  is a typical time stepping requirement that would be observed in the Earth-ionosphere waveguide at an altitude of 40 km during daytime conditions [18].

#### B. Stability Analysis

The stability analysis is not straightforward because of the nonlinearity in the update equation of the current density components [24]. The proposed algorithm requires that both stability conditions (above-mentioned Conditions 1 and 2) be satisfied to ensure numerical stability.

The first stability condition that must be met (Condition 1) is the Nyquist sampling theorem that states that the sampling frequency should be at least twice the highest frequency component (cyclotron frequency) of the signal,  $\Delta t_c < 1/2f_{ce}$ .

The second stability condition (Condition 2) may be determined through eigenvalue analysis. For this, the ordinary differential equations of (1)–(3) are collected and written into a single system as shown in the following, where  $Q$  is defined in Section II–B:

$$\begin{bmatrix} \frac{d\vec{J}_j}{dt} \\ \frac{d\vec{E}_j}{dt} \\ \frac{d\vec{H}_j}{dt} \end{bmatrix} = \begin{bmatrix} -(Q + v_j I) & \epsilon w_{pj}^2 I & O \\ -I & O & O \\ O & O & O \end{bmatrix} \begin{bmatrix} \vec{J}_j \\ \vec{E}_j \\ \vec{H}_j \end{bmatrix} + \begin{bmatrix} O \\ \frac{1}{\epsilon}(\nabla \times \vec{H}_j) \\ -\frac{1}{\mu}(\nabla \times \vec{E}_j) \end{bmatrix}. \quad (20)$$

Let

$$Y = \begin{bmatrix} \vec{J}_j \\ \vec{E}_j \\ \vec{H}_j \end{bmatrix}, \quad B = \begin{bmatrix} -(Q + v_j I) & \epsilon w_{pj}^2 I & O \\ -I & O & O \\ O & O & O \end{bmatrix} \text{ and} \\ f = \begin{bmatrix} O \\ \frac{1}{\epsilon}(\nabla \times \vec{H}_j) \\ -\frac{1}{\mu}(\nabla \times \vec{E}_j) \end{bmatrix}$$

in (20). Then, (20) can be written as follows:

$$\frac{dY}{dt} = BY + f. \quad (21)$$

Each element of  $Y$  and  $f$  is a  $3 \times 1$  matrix (to account for all vector components in the  $x$ -,  $y$ -, and  $z$ -directions). Likewise, each element of matrix  $B$  is a  $3 \times 3$  matrix.  $I$  is

an identity matrix and  $O$  is a null matrix.  $f$  is assumed to be a forcing function, whose entries are solely from Maxwell's equations (1) and (2), and as a result does not include any components from the plasma current density equation. A separate stability analysis of " $f$ " would yield the Courant stability limit (popularly known as CFL in FDTD literature). Thus, " $f$ " is ignored in our analysis.

Discretizing (21) (after ignoring  $f$ ) yields

$$\frac{Y^{n+1} - Y^n}{\Delta t_c} = B \cdot Y^n \quad (22)$$

$$Y^{n+1} = (I + B \cdot \Delta t_c)Y^n. \quad (23)$$

For stability, the error must not grow from iteration to iteration. Note that generalized time stepping is used here. Mathematically, this is written as

$$\|Y^{n+1}\| \leq \|Y^n\|. \quad (24)$$

Let

$$G = (I + B \cdot \Delta t_c). \quad (25)$$

Equation (24) only holds when the spectral radius of matrix  $G$  is less than or equal to 1, i.e.,  $\rho(G) \leq 1$ . This can be evaluated by determining the eigenvalue of matrix  $G$ , and the specific stability condition (in terms of  $\Delta t_c$ ) may be obtained by assuming the largest eigenvalue of matrix  $G$  to be less than or equal to unity. The size of matrix  $G$  is  $9 \times 9$ . Therefore, it is extremely tedious (although not impossible) to evaluate the generalized stability condition. Instead, it is recommended to manually calculate matrix  $G$  (in MATLAB, Python, and so on) using the plasma parameters and make sure that the largest eigenvalue is less than or equal to unity. The matrix  $G$  is given in Appendix C for convenience.

The stability analysis is much simpler (because of smaller matrix size) if the plasma angular frequency is 0. In this case, (7) reduces to the following:

$$\begin{bmatrix} J_x \\ J_y \\ J_z \end{bmatrix}^{n+\frac{1}{2}} = [A^{-1}]_{3 \times 3} \cdot [B]_{3 \times 3} \cdot \begin{bmatrix} J_x \\ J_y \\ J_z \end{bmatrix}^{n-\frac{1}{2}}. \quad (26)$$

For stability,  $\|J^{n+(1/2)}\| \leq \|J^{n-(1/2)}\|$  must hold for each iteration. This is only possible if the largest eigenvalue of  $[A^{-1}]_{3 \times 3} \cdot [B]_{3 \times 3}$  is less than or equal to unity.

#### IV. MEMORY REQUIREMENTS

As stated in Section I, the algorithm of [6] is severely memory intensive in exchange for providing a time step increment that does not depend on the plasma parameters. In this Section, the memory requirements of [3] and [5] are compared with the algorithm proposed in this paper. The algorithm of [12] and the method proposed in this paper (for the case of  $\Delta t_c = \Delta t$ ) have identical memory requirements, so the method of [12] is not included in the comparison.

The anisotropic model of [3] requires six real numbers for the  $\vec{H}$  and  $\vec{E}$  components (three each), 12 real coefficients (six per  $\vec{H}$  and  $\vec{E}$  field components),  $3(1+n)$  real numbers for the  $\vec{J}_j$  components (electrons and  $n$ -ion species, such as  $O^+$ ,  $N^+$ , and so on), and  $4 \times ((6+3n) \times (6+3n))$  real

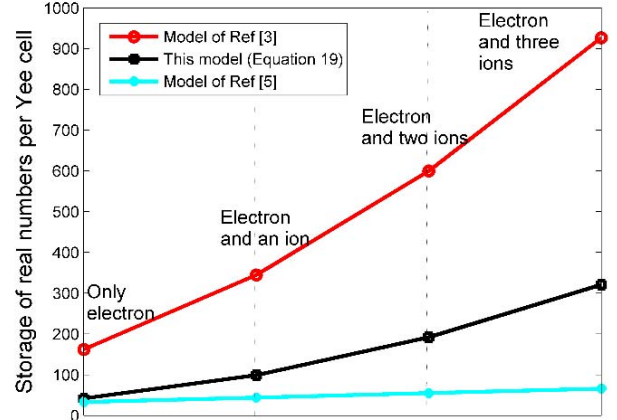


Fig. 4. Comparison of the memory requirements per Yee grid cell for this proposed model (19) with two previous anisotropic models (red line for [3] and light blue line for [5]). Note that the memory requirements for (7) and (18) are not shown here as both occupy just three real numbers less than (19).

numbers for the four coefficient matrices ( $A$ ,  $A^{-1}$ ,  $B$ , and  $C$ ). Therefore, the anisotropic plasma of [3], including electrons and  $n$ -ion species, requires the storage of  $18+3n+4(6+3n)^2$  real numbers within each Yee grid cell.

The anisotropic model of [5] is more memory efficient. It requires the same memory as in [3] to store the  $\vec{E}$  and  $\vec{H}$  fields and their updating coefficients. Then, it requires  $3(1+n)$  real numbers for the  $\vec{J}_j$  components and  $2(3+n)$  numbers for  $\vec{s}$  and  $\vec{r}$ . In addition, it requires  $6(1+n)$  real numbers for predictor and corrector  $\vec{J}_j$  components. Overall, this model requires storage of  $33+11n$  real numbers within each Yee grid cell.

The anisotropic plasma model proposed here (for the case of  $\Delta t_c = \Delta t$ ) requires the same memory as in [3] and [5] to store the  $\vec{E}$  and  $\vec{H}$  fields and their updating coefficients. Then, it requires  $3(1+n)$  real numbers for the  $\vec{J}_j$  components along with  $2 \times ((3+3n) \times (3+3n))$  real coefficients to store the two coefficient matrices ( $\epsilon \cdot \Delta t_c \cdot w_{pj}^2 \cdot [A^{-1}]_{3 \times 3}$  and  $A^{-1}B$ ). When implementing (18), it requires  $2 \times ((3+3n) \times (3+3n))$  real coefficients to store the results of  $([I]_{3 \times 3} + \sum_{k=1}^{M-2} ([A^{-1}]_{3 \times 3} [B]_{3 \times 3})^k) \cdot \epsilon \cdot \Delta t_c \cdot w_{pj}^2 \cdot [A^{-1}]_{3 \times 3}$  and  $([A^{-1}]_{3 \times 3} [B]_{3 \times 3})^{M-1}$  so that they can be precomputed at the beginning of simulation. Finally, when implementing (19), three more real numbers are needed to store the past values of the electric field. Therefore, to model plasma anisotropy with electron and  $n$ -ion species, this model (19) requires  $21+3+3n+2(3+3n)^2$  real numbers.

This memory requirement for the proposed algorithm is much less than for the model in [3], as shown in Fig. 4. Compared to the model in [5], the memory requirement is slightly higher when modeling only electrons, but the difference grows more when modeling ions. In Fig. 5, when including only electrons, the model reported in [3] requires 162 real numbers per grid cell, the model reported in [5] requires 33 real numbers, and the proposed method of this paper requires 39, 39, and 42 real numbers per grid cell for the following three cases, respectively:  $\Delta t_c = \Delta t$ ,  $\Delta t_c < \Delta t$  using a singular update of  $\vec{J}$  each  $\Delta t$ , and  $\Delta t_c < \Delta t$  using three updates of  $\vec{J}$  each  $\Delta t$ .

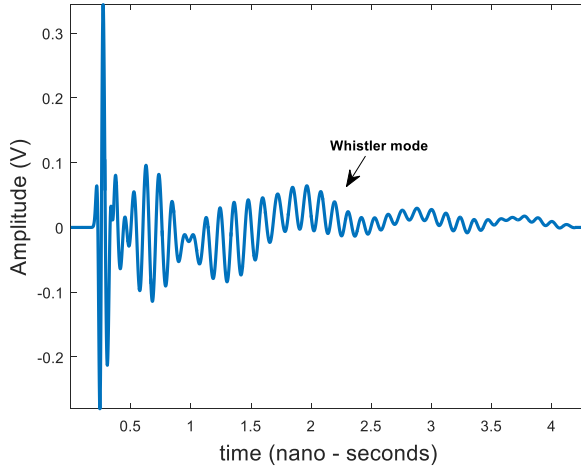


Fig. 5. Time-waveform of an  $E_x$  field component 40 cells into the magnetized plasma.

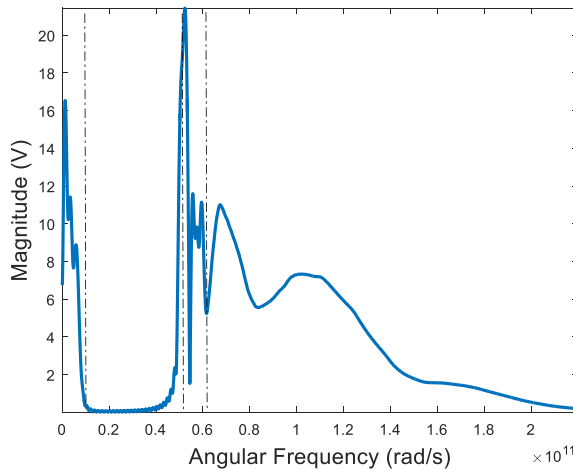


Fig. 6. Spectrum of the recorded time-waveform of Fig. 6. The three dotted lines mark the cyclotron frequency, cutoff frequency for the L-wave, and the cutoff frequency for the R-wave.

While testing all of these algorithms, the real numbers are stored in double-precision floating-point format for better accuracy, which requires 64 bits of memory per real number. Therefore, when modeling only electrons, the model of [3] requires 1.26 kB/s of memory per Yee cell, the model reported in [5] occupies 0.26 kB/s of memory per cell, and the model reported in this paper requires 0.31, 0.31, and 0.33 kB/s of memory per cell for  $\Delta t_c = \Delta t$ ,  $\Delta t_c < \Delta t$  when using a singular update of  $\vec{J}$  each  $\Delta t$ , and  $\Delta t_c < \Delta t$  when using three updates of  $\vec{J}$  each  $\Delta t$ , respectively.

## V. CONCLUSION

A new FDTD algorithm has been proposed to model EM wave propagation in anisotropic magnetized plasma. The primary advantages of this model are as follows.

- 1) This method is straightforward to implement and it is not memory intensive, especially compared to the approach presented in [6].
- 2) Two different time step increments may be chosen, one for Maxwell's equations and the other for the current density equation.
- 3) Even when the time step increment for the current density equation is smaller than the Courant limit for

Maxwell's equations, only a single update at each time step is needed for (3).

This proposed model is validated against several analytical plasma theory results, as shown in Appendix B. The performance of the new algorithm is compared with the previous approaches. For the first time, a complete stability condition using eigenvalue analysis is presented. From this analysis, efficient time step increments may be chosen for varying modeling scenarios and plasma compositions.

## APPENDIX

### A. Matrix Representation

The matrix representations of A and B are as follows:

$$A = \begin{bmatrix} a & -\frac{\Delta t_c}{2}\omega_z & \frac{\Delta t_c}{2}\omega_y \\ \frac{\Delta t_c}{2}\omega_z & a & -\frac{\Delta t_c}{2}\omega_x \\ -\frac{\Delta t_c}{2}\omega_y & \frac{\Delta t_c}{2}\omega_x & a \end{bmatrix}$$

$$B = \begin{bmatrix} b & \frac{\Delta t_c}{2}\omega_z & -\frac{\Delta t_c}{2}\omega_y \\ -\frac{\Delta t_c}{2}\omega_z & b & \frac{\Delta t_c}{2}\omega_x \\ \frac{\Delta t_c}{2}\omega_y & -\frac{\Delta t_c}{2}\omega_x & b \end{bmatrix}.$$

### B. Validations

In all of the following validation tests, the number of grid cells in the  $x$ -,  $y$ -, and  $z$ -directions are sufficiently large ( $600 \times 600 \times 600$  cells) to avoid any reflections from the grid edges. Thus, the computational domain is truncated by a perfectly electrical conductor. The plasma is modeled with an electron density of  $1.0 \times 10^{18} \text{ m}^{-3}$ . The electron plasma angular frequency is  $5.64 \times 10^{10} \text{ rad/s}$ . The excitation is an  $x$ -polarized sinusoidal plane source propagating in the  $z$ -direction.

1) *Validation 1:* For the first set of validation tests, an  $x$ -polarized and  $z$ -directed plane wave Gaussian source is used. The source time-waveform is

$$E_x = \exp\left(-\frac{(t-50\Delta t)^2}{2(7\Delta t)^2}\right). \quad (27)$$

Initially, the electrons are subjected to an applied magnetic field intensity of 0.06 T. The applied field is polarized in the  $z$ -direction (parallel to the direction of propagation). The spatial grid resolution is  $\Delta x = \Delta y = \Delta z = 1 \text{ mm}$ . The time steps ( $\Delta t$  and  $\Delta t_c$ ) are identical and equal to 1.905 ps.

Figs. 5 and 6 illustrate the time-domain electric field (see Fig. 5) and its spectrum (see Fig. 6) recorded 40 cells into the plasma (away from the source). The Gaussian pulse is observed to excite an R-wave, an L-wave, and a low-frequency whistler-mode wave. The sharp cutoff frequency for the L- and R-waves is observed in Fig. 6. The analytical frequencies for an electron density of  $10^{18} \text{ electrons/m}^3$  are as follows:

- 1) electron cyclotron frequency:  $1.06 \times 10^{10} \text{ rad/s}$ ;
- 2) cutoff frequency for L-wave:  $5.14 \times 10^{10} \text{ rad/s}$ ;
- 3) cutoff frequency for R-wave:  $6.19 \times 10^{10} \text{ rad/s}$ .

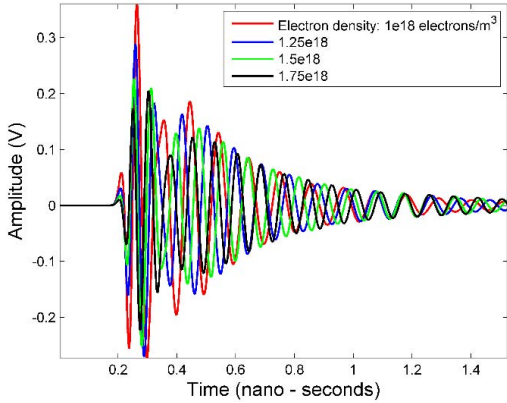


Fig. 7. Time-domain waveforms of a Gaussian-pulse plane wave-sourced EM wave propagating in a plasma medium having different electron densities in the absence of an externally applied magnetic field.

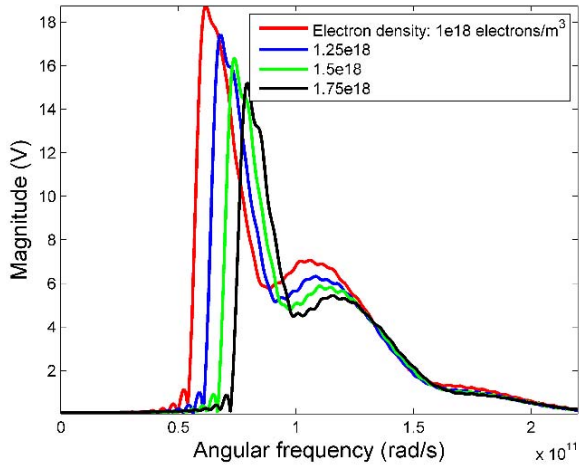


Fig. 8. Corresponding frequency-domain waveforms of the time-domain waveforms shown in Fig. 7.

Figs. 7 and 8 then illustrate the time-domain electric field (see Fig. 7) and the corresponding spectrum (see Fig. 8) sampled at the same spatial position as for Fig. 5 but for different cases of electron densities now in the absence of an externally applied magnetic field. The results in Figs. 7 and 8 are used to study the numerical error for different electron densities in the plasma medium. It is found out that there is a strong agreement between the simulated and analytical plasma frequencies. The average error for all of these cases is 0.524%. The error is determined by

$$\text{Error(in\%)} = \frac{|\omega_{\text{PJA}} - \omega_{\text{PJS}}|}{\omega_{\text{PJA}}} \times 100 \quad (28)$$

where  $\omega_{\text{PJA}}$  and  $\omega_{\text{PJS}}$  denote the analytical plasma angular frequency and the simulated plasma angular frequency, respectively. In Fig. 8, the simulated plasma angular frequency is obtained at the halfway point (horizontally) between the minimum and maximum points (vertically). The tabular data are provided in Table II.

2) *Validation 2*: The second validation test demonstrates the Faraday rotation effect of a magnetized plasma. According to plasma theory, an initially linearly polarized sinusoidal wave at a frequency above the right-hand circularly polarized wave (R-wave) and left-hand circularly polarized wave (L-wave) cutoff frequencies begins to rotate as it propagates through a mag-

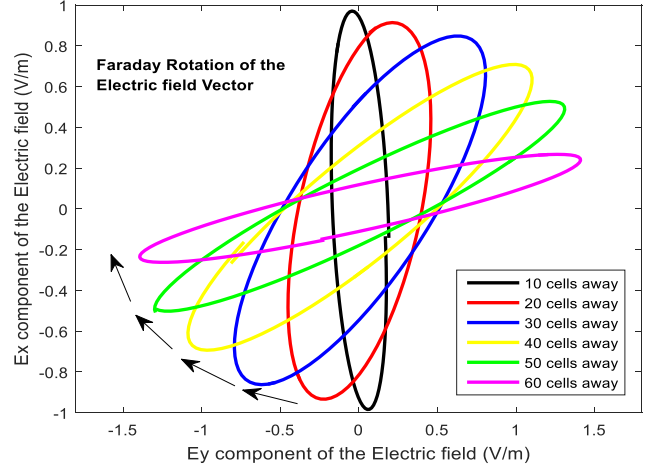


Fig. 9. Faraday rotation effect recorded at varying distances along the z-direction (parallel with the applied magnetic field) away from an x-polarized sinusoidal plane wave source.

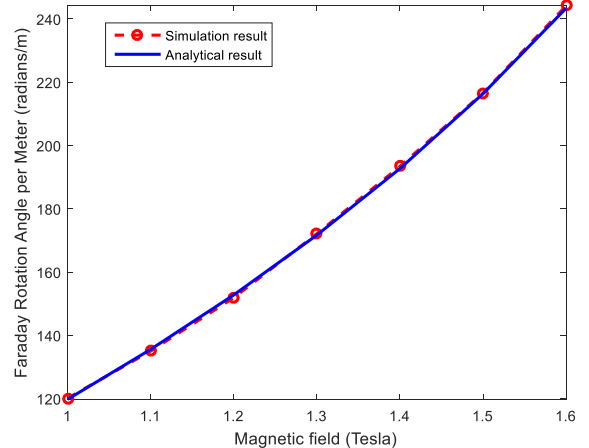


Fig. 10. Comparison of the simulated (red curve) and analytical results (blue curve) for the Faraday rotation angle per meter.

netized plasma. This is called “Faraday rotation.” Specifically, the initially linearly polarized wave decomposes into right-hand and left-hand circularly polarized waves that propagate with different phase velocities in the plasma.

A magnetic field intensity of 1.7 T polarized in the z-direction is applied for this validation test. The sinusoidal plane wave of source frequency  $5.718 \times 10^{11}$  rad/s is sent into the plasma. The spatial grid resolution is again  $\Delta x = \Delta y = \Delta z = 75 \mu\text{m}$ . The time steps ( $\Delta t$  and  $\Delta t_c$ ) are identical and equal to 0.1428 ps. The electric fields along x- and y-directions at varying distances away from the source are plotted in Fig. 9.

3) *Validation 3*: For the third validation, the amount of Faraday rotation is tested for several magnetic field intensities. During rotation, the expected rotation angle per unit distance  $\theta_{\text{FA}}$  is  $\theta_{\text{FA}} = ((\beta_{\text{LH}} - \beta_{\text{RH}})/2)$ . The propagation constants ( $\beta_{\text{LH}}$  and  $\beta_{\text{RH}}$ ) are given by the following expressions:

$$\beta_{\text{LH}} = \omega(\mu\epsilon)^{1/2} \sqrt{1 - \frac{\frac{\omega_{\text{pe}}^2}{\omega}}{\omega_{\text{ce}} + \omega}} \quad (29)$$

$$\beta_{\text{RH}} = \omega(\mu\epsilon)^{1/2} \sqrt{1 - \frac{\frac{\omega_{\text{pe}}^2}{\omega}}{\omega_{\text{ce}} - \omega}} \quad (30)$$

TABLE II  
DATA RELATED TO ERROR ANALYSIS WITH RESPECT TO THE CHANGE IN ELECTRON DENSITY

Electron density (electrons/m <sup>3</sup> )	Analytical plasma angular frequency ( $\omega_{PJA}$ ) in rad/sec	Simulated mean plasma angular frequency ( $\omega_{PJS}$ ) in rad/sec	Error (in %) $\frac{ \omega_{PJA} - \omega_{PJS} }{\omega_{PJA}} \times 100$
$1.0 \times 10^{18}$	$5.638 \times 10^{10}$	$5.6925 \times 10^{10}$	0.96
$1.25 \times 10^{18}$	$6.3035 \times 10^{10}$	$6.337 \times 10^{10}$	0.53
$1.5 \times 10^{18}$	$6.9052 \times 10^{10}$	$6.9305 \times 10^{10}$	0.36
$1.75 \times 10^{18}$	$7.4584 \times 10^{10}$	$7.477 \times 10^{10}$	0.249

TABLE III  
DATA RELATED TO ERROR ANALYSIS WITH RESPECT TO THE CHANGE IN MAGNETIC FIELD INTENSITY

B <sub>z</sub> (Magnetic field intensity in Tesla) oriented in z-axis	Analytical Faraday rotation ( $\theta_{FA}$ ) in degrees	Simulated Faraday rotation ( $\theta_{FS}$ ) in degrees	Error (in %) $\frac{ \theta_{FS} - \theta_{FA} }{\theta_{FA}} \times 100$
1	119.7656	120.1178	0.294
1.1	135.5671	135.0298	0.396
1.2	152.7654	151.8855	0.577
1.3	171.6791	172.1105	0.251
1.4	192.7029	193.4049	0.364
1.5	216.3661	216.56	0.089
1.6	243.3818	244.1777	0.327

where  $\omega$ ,  $\omega_{pe}$ , and  $\omega_{ce}$  represent the frequency of the linearly polarized plane wave, the plasma frequency, and the cyclotron frequency of the electrons, respectively.

The spatial grid resolution is set to  $\Delta x = \Delta y = \Delta z = 75 \mu\text{m}$ . The time steps ( $\Delta t$  and  $\Delta t_c$ ) are identical and equal to 0.1428 ps. Several simulations are run, each using a different geomagnetic intensities (ranging from 1 to 1.6 T). The rotation angle per unit distance is measured in the FDTD simulation using  $\theta_{FS} = ((\tan^{-1}(\frac{E_y}{E_z})))/d$ .

A comparison between the simulation and analytical results for the rotation angle per unit distance is shown in Fig. 10.

There is a strong agreement between the two sets of results. The average error is 0.328%. The error is determined by

$$\text{Error (in\%)} = \frac{|\theta_{FS} - \theta_{FA}|}{\theta_{FA}} \times 100 \quad (31)$$

where  $\theta_{FA}$  and  $\theta_{FS}$  denote the analytical Faraday rotation and simulated Faraday rotation, respectively. The tabular data are given in Table III.

### C. Matrix Representation

The matrix G is shown as the bottom of this page.

$$G = \begin{bmatrix} 1 - v_j \Delta t_c & \omega_z \Delta t_c & -\omega_y \Delta t_c & \varepsilon \omega_{pj}^2 \Delta t_c & 0 & 0 & 0 & 0 & 0 \\ -\omega_z \Delta t_c & 1 - v_j \Delta t_c & \omega_x \Delta t_c & 0 & \varepsilon \omega_{pj}^2 \Delta t_c & 0 & 0 & 0 & 0 \\ \omega_y \Delta t_c & -\omega_x \Delta t_c & 1 - v_j \Delta t_c & 0 & 0 & \varepsilon \omega_{pj}^2 \Delta t_c & 0 & 0 & 0 \\ -\Delta t_c & 0 & 0 & 1 & 0 & 0 & 0 & 0 & 0 \\ 0 & -\Delta t_c & 0 & 0 & 1 & 0 & 0 & 0 & 0 \\ 0 & 0 & -\Delta t_c & 0 & 0 & 1 & 0 & 0 & 0 \\ 0 & 0 & 0 & 0 & 0 & 0 & 1 & 0 & 0 \\ 0 & 0 & 0 & 0 & 0 & 0 & 0 & 1 & 0 \\ 0 & 0 & 0 & 0 & 0 & 0 & 0 & 0 & 1 \end{bmatrix}$$

## D. Error Data

See Tables II and III.

## ACKNOWLEDGMENT

The authors would like to thank the Extreme Science and Engineering Discovery Environment for providing supercomputing resources (EAR140019) as well as the Center for High Performance Computing, The University of Utah.

## REFERENCES

- [1] K. Yee, "Numerical solution of initial boundary value problems involving Maxwell's equations in isotropic media," *IEEE Trans. Antennas Propag.*, vol. AP-14, no. 3, pp. 302–307, May 1966.
- [2] A. Taflove and S. C. Hagness, *Computational Electrodynamics: The Finite-Difference Time-Domain Method*, 3rd ed. Norwood, MA, USA: Artech House, 2005.
- [3] Y. Yu and J. J. Simpson, "An E-J collocated 3-D FDTD model of electromagnetic wave propagation in magnetized cold plasma," *IEEE Trans. Antennas Propag.*, vol. 58, no. 2, pp. 469–478, Feb. 2010.
- [4] Y. Yu, J. Niu, and J. J. Simpson, "A 3-D global Earth-ionosphere FDTD model including an anisotropic magnetized plasma ionosphere," *IEEE Trans. Antennas Propag.*, vol. 60, no. 7, pp. 3246–3256, Jul. 2012.
- [5] A. Samimi and J. J. Simpson, "An efficient 3-D FDTD model of electromagnetic wave propagation in magnetized plasma," *IEEE Trans. Antennas Propag.*, vol. 63, no. 1, pp. 269–279, Jan. 2015.
- [6] E. Gamliel, "Direct integration 3-D FDTD method for single-species cold magnetized plasma," *IEEE Trans. Antennas Propag.*, vol. 65, no. 1, pp. 295–308, Jan. 2017.
- [7] J. L. Young, "A full finite difference time domain implementation for radio wave propagation in a plasma," *Radio Sci.*, vol. 29, no. 6, pp. 1513–1522, 1994.
- [8] J. L. Young, "A higher order FDTD method for EM propagation in a collisionless cold plasma," *IEEE Trans. Antennas Propag.*, vol. 44, no. 9, pp. 1283–1289, Sep. 1996.
- [9] S. A. Cummer, "An analysis of new and existing FDTD methods for isotropic cold plasma and a method for improving their accuracy," *IEEE Trans. Antennas Propag.*, vol. 45, no. 3, pp. 392–400, Mar. 1997.
- [10] M. Thèvenot, J.-P. Bérenger, T. Monedièvre, and F. Jecko, "A FDTD scheme for the computation of VLF-LF propagation in the anisotropic earth-ionosphere waveguide," *Ann. Telecommun.*, vol. 54, pp. 297–310, May 1999, doi: [10.1007/BF02995540](https://doi.org/10.1007/BF02995540).
- [11] C. K. Birdsall and A. B. Langdon, *Plasma Physics Via Computer Simulation*. New York, NY, USA: IoP, 1991.
- [12] J. H. Lee and D. K. Kalluri, "Three-dimensional FDTD simulation of electromagnetic wave transformation in a dynamic inhomogeneous magnetized plasma," *IEEE Trans. Antennas Propag.*, vol. 47, no. 7, pp. 1146–1151, Jul. 1999.
- [13] P. Li and L. J. Jiang, "Simulation of electromagnetic waves in the magnetized cold plasma by a DG-FDTD method," *IEEE Antennas Wireless Propag. Lett.*, vol. 12, pp. 1244–1247, 2013.
- [14] J. Cao, D. Ding, G. Cheng, and R. Chen, "A higher order Nyström TD-VIE method for scattering from magnetized plasma objects," *IEEE Antennas Wireless Propag. Lett.*, vol. 16, pp. 408–411, 2017.
- [15] J. J. Simpson and A. Taflove, "Three-dimensional FDTD modeling of impulsive ELF propagation about the Earth-sphere," *IEEE Trans. Antennas Propag.*, vol. 52, no. 2, pp. 443–451, Feb. 2004.
- [16] J. J. Simpson, "Current and future applications of full-vector 3-D Maxwell's equations FDTD global Earth-ionosphere waveguide models," *Surv. Geophys.*, vol. 30, no. 2, pp. 105–130, 2009.
- [17] J. J. Simpson and A. Taflove, "ELF radar system proposed for localized D-region ionospheric anomalies," *IEEE Geosci. Remote Sens. Lett.*, vol. 3, no. 4, pp. 500–503, Oct. 2006.
- [18] M. Hayakawa and T. Otsuyama, "FDTD analysis of ELF wave propagation in inhomogeneous subionospheric waveguide models," *Appl. Comput. Electromagn. J.*, vol. 17, no. 3, pp. 239–244, 2002.
- [19] A. Samimi and J. J. Simpson, "Parallelization of 3-D global FDTD Earth-ionosphere waveguide models at resolutions on the order of  $\sim 1$  km and higher," *IEEE Antennas Wireless Propag. Lett.*, vol. 15, pp. 1959–1962, 2016.
- [20] S. Pokhrel, M. Rodriguez, A. Samimi, G. Heber, and J. Simpson, "Parallel I/O for 3-D global FDTD Earth-ionosphere waveguide models at resolutions on the order of  $\sim 1$  km and higher using HDF5," *IEEE Trans. Antennas Propag.*, to be published, doi: [10.1109/TAP.2018.2835163](https://doi.org/10.1109/TAP.2018.2835163).
- [21] J. P. Boris, "The acceleration calculation from a scalar potential," Plasma Phys. Lab., Princeton Univ., Princeton, NJ, USA, Tech. Rep. MATT-152, Mar. 1970.
- [22] W. Hu and S. A. Cummer, "An FDTD model for low and high altitude lightning-generated EM fields," *IEEE Trans. Antennas Propag.*, vol. 54, no. 5, pp. 1513–1522, May 2006.
- [23] W. Hu, S. A. Cummer, and W. A. Lyons, "Testing sprite initiation theory using lightning measurements and modeled electromagnetic fields," *J. Geophys. Res., Atmos.*, vol. 112, pp. 12645–12656, Jul. 2007.
- [24] F. F. Chen, *Introduction to Plasma Physics and Controlled Fusion: Plasma Physics*, 2nd ed. New York, NY, USA: Springer, 1984.



**Santosh Pokhrel** (S'16) received the bachelor's degree in electronics and communication engineering from Jawaharlal Nehru Technological University at Kakinada, Kakinada, India, in 2015. He is currently pursuing the Ph.D. degree with the Electrical and Computer Engineering Department, The University of Utah, Salt Lake City, UT, USA.

His current research interests include finite-difference time-domain solution of Maxwell's equations and its applications in investigating space weather hazards to electric power grids, numerical modeling of engineering problems, and design of analog ICs.



**Varun Shankar** is currently an Assistant Professor Lecturer with the Department of Mathematics, The University of Utah, Salt Lake City, UT, USA, where he is a member of the Applied Mathematics Group and the Math Biology Group. His current research interests include in developing numerical methods for the simulation of mathematical models of biological systems, the development of efficient and stable high-order meshfree numerical methods based on the radial basis function interpolation for the solution of partial differential equations on irregular domains programming, and machine learning.



**Jamesina J. Simpson** (S'01–M'07–SM'12) received the B.S. and Ph.D. degrees in electrical engineering from Northwestern University, Evanston, IL, USA, in 2003 and 2007, respectively.

She is currently an Associate Professor with the Electrical and Computer Engineering Department, The University of Utah, Salt Lake City, UT, USA. Her research lab encompasses the application of the full-vector Maxwell's equations finite-difference time-domain method to electromagnetic wave propagation spanning 15 orders of magnitude across the electromagnetic spectrum.

Dr. Simpson received the 2010 National Science Foundation Career Award, the 2012 Donald G. Dudley, Jr., Undergraduate Teaching Award of the IEEE Antennas and Propagation Society, and the Santimay Basu Medal from the International Union of Radio Science in 2017.